ELSEVIER

Catalysis Today 62 (2000) 303–318

CATALYSIS TODAY

www.elsevier.com/locate/cattod

The effect of oxygen concentration on the reduction of NO with propylene over CuO/γ-Al_2O_3

Yawu Chi, Steven S.C. Chuang*

Department of Chemical Engineering, The University of Akron, Akron, OH 44325-3906, USA

Abstract

The effect of oxygen concentration on the pulse and steady-state selective catalytic reduction (SCR) of NO with C_3H_6 over CuO/γ-Al_2O_3 has been studied by infrared spectroscopy (IR) coupled with mass spectroscopy studies. IR studies revealed that the pulse SCR occurred via (i) the oxidation of Cu^0/Cu^+ to Cu^{2+} by NO and O_2, (ii) the co-adsorption of $NO/NO_2/O_2$ to produce $Cu^{2+}(NO_3^-)_2$, and (iii) the reaction of $Cu^{2+}(NO_3^-)_2$ with C_3H_6 to produce N_2, CO_2, and H_2O. Increasing the O_2/NO ratio from 25.0 to 83.4 promotes the formation of NO_2 from gas phase oxidation of NO, resulting in a reactant mixture of $NO/NO_2/O_2$. This reactant mixture allows the formation of $Cu^{2+}(NO_3^-)_2$ and its reaction with the C_3H_6 to occur at a higher rate with a higher selectivity toward N_2 than the low O_2/NO flow. Both the high and low O_2/NO steady-state SCR reactions follow the same pathway, proceeding via adsorbed C_3H_7–NO_2, C_3H_7–ONO, CH_3COO^-, Cu^0–CN, and Cu^+–NCO intermediates toward N_2, CO_2, and H_2O products. High O_2 concentration in the high O_2/NO SCR accelerates both the formation and destruction of adsorbates, resulting in their intensities similar to the low O_2/NO SCR at 523–698 K. High O_2 concentration in the reactant mixture resulted in a higher rate of destruction of the intermediates than low O_2 concentration at temperatures above 723 K.

Keywords: NO reduction; O_2 effect; Reaction mechanism; Propylene pulse; NO/O_2 adsorption; Nitrate formation; Selective catalytic reduction; Infrared spectroscopy; CuO/γ-Al_2O_3

1. Introduction

Selective catalytic reduction (SCR) of NO with hydrocarbons has been a subject of extensive studies due to its potential for the effective control of NO emission in the oxidizing environment [1–15]. Catalyst screening studies have shown that supported Cu catalysts exhibit the activity for the SCR, but lack the selectivity for the efficient conversion of NO to N_2 in a wide temperature range [7,8,14]. A critical issue that needs to be addressed is the control of catalyst activity and selectivity.

The concentration of O_2 in the NO-containing stream plays an important role in the reaction rate and product selectivity of the SCR [15–34]. It has been suggested that the roles of O_2 in the NO SCR are: (i) to activate NO and hydrocarbons [23]; (ii) to oxidize NO to NO_2 [26]; (iii) to maintain a Cu^+/Cu^{2+} site balance [24]; and (iv) to react with carbonaceous deposits on Cu–ZSM-5 [25–27]. A number of studies have proposed that the NO–O_2–C_3H_6 reaction proceeds via: (i) NO_2 as an intermediate which further reacts with hydrocarbons on Ce–ZSM-5 [26] and Cu–ZSM-5 [27]; (ii) a partially oxidized intermediate on H-Zeolite and Al_2O_3 [28] and Cu–ZSM-5 [29]; and (iii) adsorbed NO_x on Al_2O_3 and Ag/Al_2O_3 [14], Ag/TiO_2–ZrO_2 [30], Al_2O_3 [31], Cu–ZSM-5 [32].

* Corresponding author. Tel.: +1-330-972-6993; fax: +1-330-972-5856.
E-mail address: schuang@uakron.edu (S.S.C. Chuang).

0920-5861/00/$ – see front matter
PII: S0920-5861(00)00432-6

Our recent study [34] on $CuO/\gamma\text{-}Al_2O_3$ has shown that the product selectivity, the catalyst surface state, and its adsorbates are strongly influenced by the steady-state and the pulse reaction conditions. Under the steady-state conditions, $NO/O_2/C_3H_6$ adsorbed as C_3H_7–NO_2, CH_3COO^-, Cu^+–NCO, Cu^0–CN, Cu^+–CO species and further reacted to produce N_2, CO_2, and H_2O. Under the conditions of pulsing C_3H_6 into the NO/O_2 stream, NO/O_2 adsorbed as $(NO_3^-)_2$ which further reacted with the C_3H_6 pulse to produce N_2, N_2O, CO_2, and H_2O. Conditions for pulsing C_3H_6 into the NO/O_2 stream resemble those proposed mode of operation which involves NO/O_2 adsorption followed by the pulse hydrocarbon reduction for the removal of NO_x emission from the lean-burn and diesel engines [33].

The development of catalysts for the effective removal of NO_x from various oxygen-containing NO_x streams of coal-fired plant, lean-burn, and diesel engine emissions requires a fundamental understanding of the role of oxygen in the SCR reaction. To further elucidate the effect of O_2 concentration on the reaction rate and selectivity, the catalyst surface state, and its adsorbates, we have studied the steady-state SCR and the pulse SCR with C_3H_6 under a high O_2/NO flow and a low O_2/NO flow. The high O_2/NO flow consisted of 0.08% NO + 6.67% O_2 + 93.25% He of which the O_2/NO ratio is in the range of the exhaust composition of coal-fired power plant. The low O_2/NO flow consisted of 0.08% NO + 2% O_2 + 97.92% He of which the O_2/NO ratio is close to that of lean burn engine emission.

2. Experimental

2.1. Catalyst precursor preparation and XRD characterization

$Cu(NO_3)_2{\cdot}H_2O/\gamma\text{-}Al_2O_3$ was prepared by impregnation of $\gamma\text{-}Al_2O_3$ (Alfa products, SA: 100 m^2/g, pore size: 0.01-0.02 μm) using $Cu(NO_3)_2{\cdot}3H_2O$ (Strem chemicals) solution. The Cu loading on the catalyst is 2.7 wt.%. The resulting sample was dried overnight in air at 298 K. One hundred milligrams of the catalyst powder was pressed into three self-supporting disks. One disk was placed in the IR beam path in the IR cell; the other two disks were broken down into flakes and placed in vicinity of the self-supporting disk to increase the conversion of reactants and to obtain a strong mass spectrometer (MS) signal for the composition analysis of the reactor effluent [34,35]. Prior to adsorption and reaction studies, $Cu(NO_3)_2{\cdot}H_2O/\gamma\text{-}Al_2O_3$ was thermally decomposed to $CuO/\gamma\text{-}Al_2O_3$ at 773 K in flowing He. X-ray diffraction (XRD) study of $CuO/\gamma\text{-}Al_2O_3$ by using CuKα radiation did not produce any diffraction pattern for CuO or CuO_x, suggesting that Cu oxide is highly dispersed on $\gamma\text{-}Al_2O_3$. The total number of Cu^{2+}, Cu^+, and Cu^0 on the surface of $\gamma\text{-}Al_2O_3$ was determined to be 25 μmol/g of $CuO/\gamma\text{-}Al_2O_3$ by pulse CO adsorption at 298 K, assuming $CO/Cu_{site} = 1$. Prior to each experiment, the $CuO/\gamma\text{-}Al_2O_3$ catalyst was pretreated in He flow at 773 K for 1 h and cooled to the desired temperature.

2.2. NO/O_2 adsorption on $CuO/\gamma\text{-}Al_2O_3$

NO/O_2 adsorption studies were carried out by flowing (i) a low O_2/NO ratio (0.08% NO + 2% O_2 + 97.92% He, $O_2/NO = 25.0$) flow, and (ii) a high O_2/NO ratio (0.08% NO + 6.67% O_2 + 93.25% He, $O_2/NO = 83.4$) flow at a total flow rate of 75 cm^3/min over $CuO/\gamma\text{-}Al_2O_3$ at 298, 523, 623, and 723 K. 1.01% NO with He balance (Praxair), 99.99% O_2 (Praxair), 99.999% He (Praxair), and C_3H_6 (LINDE Specialty Gas) were used. These reactant feed were prepared by mixing 1.01% NO, 99.99% O_2, and 99.999% He flow. The high O_2/NO ratio promotes the reaction between O_2 and NO to produce NO_2 in the high O_2/NO flow at 298 K, changing its initial composition to 0.05% NO + 0.03% NO_2 + 6.66% O_2 + 93.26% He. Fig. 1 shows the IR spectra of the high and low O_2/NO ratio flow and lists the compositions of the reactant stream at 298 K.

2.3. Pulsing C_3H_6 into the steady-state NO/O_2 flow over $CuO/\gamma\text{-}Al_2O_3$ and the steady-state SCR reaction of $NO/O_2/C_3H_6$ over $CuO/\gamma\text{-}Al_2O_3$

Upon both adsorbate and reactant/product concentrations reaching the steady-state during a constant NO/O_2 flow, selective catalytic reduction (SCR) of NO was carried out by pulsing three consecutive 1 cm^3 of C_3H_6 into either high or low O_2/NO flow at 0.1 MPa and 523, 623, and 723 K. Three consecutive pulses of

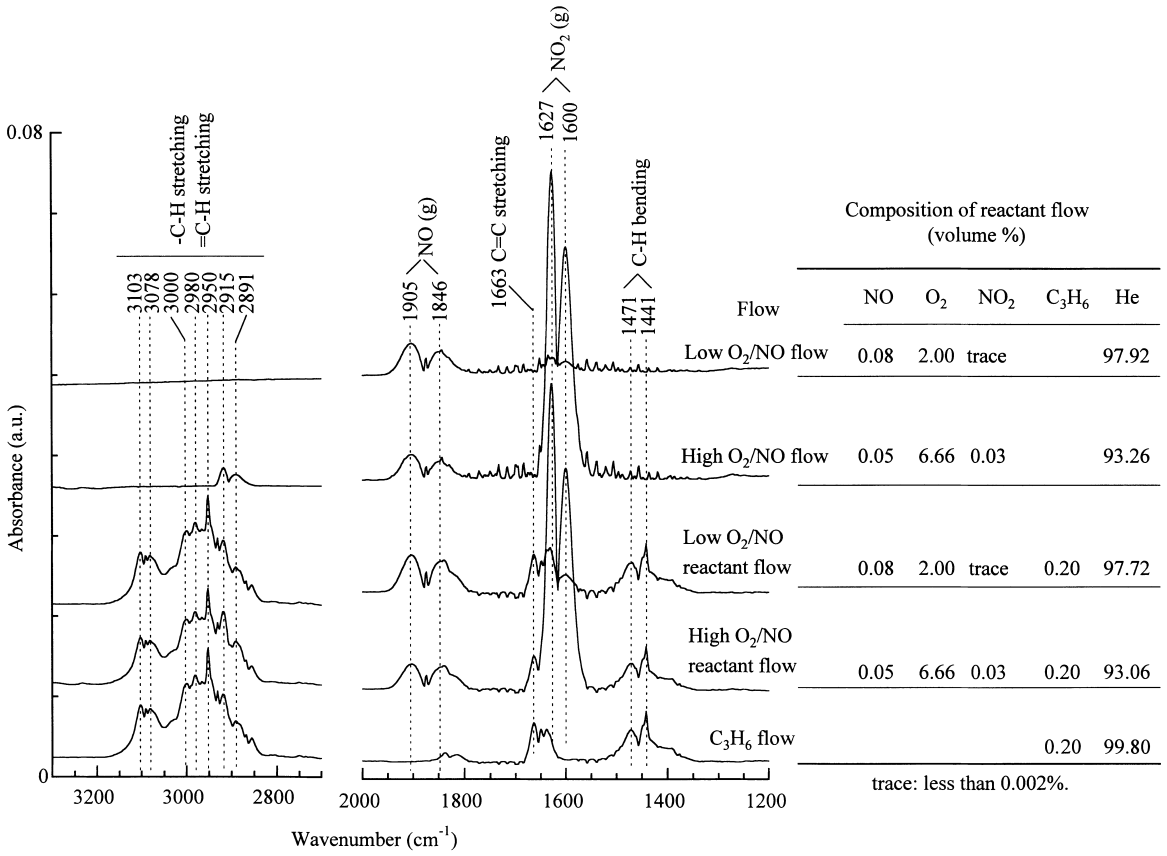

Fig. 1. IR spectra and the composition of the inlet reactant flow at 298 K.

1 cm^3 C_3H_6 were used in the SCR of NO to result in an appreciable conversion of NO, as shown by decrease in the NO concentration profile in Figs. 4–6. The extent of decrease in the NO profile reflects that of NO conversion. However, NO conversion cannot be easily estimated due to the difficulty in calibrating the decreasing NO profile. The amount of products (N_2, N_2O, and CO_2) formed during C_3H_6 pulse was calculated using the area under each MS profiles. A good agreement in carbon balance between C_3H_6 conversion and CO_2 formation was achieved.

Steady-state SCR reactions of the high O_2/NO reactant flow (0.05% NO+0.03% NO_2+6.66% O_2+0.2% C_3H_6 + 93.06% He) and the low O_2/NO reactant flow (0.08% NO + 2% O_2 + 0.2% C_3H_6 + 97.72% He) on CuO/γ-Al_2O_3 were carried out to determine the effect of O_2 concentration on SCR at 0.1 MPa, and 523, 623, 673, 698, 723, and 773 K.

2.4. Infrared spectroscopy and mass spectrometer

Variation in adsorbate concentration was determined by a Nicolet 5SCX and a Nicolet 550-Magna FTIR spectrometers (IR) at a 4-cm^{-1} resolution with 32 co-added scans. Variation in reactant/product concentration was determined by a Balzers QMG 112 and a Prisma QMS 200 mass spectrometer (MS) (Pfeiffer Vacuum Technology). The mass-to-charge ratios (*m*/*e*, i.e. amu) for MS monitoring were $m/e = 4$ for He; $m/e = 18$ for H_2O; $m/e = 28$ for N_2 and CO; $m/e = 12$ (CO fragment) for separation of CO from $m/e = 28$; $m/e = 30$ for NO; $m/e = 32$ for O_2; $m/e = 44$ for N_2O and CO_2; $m/e = 22$ (CO_2 double ionization) for separation of CO_2 from $m/e = 44$; $m/e = 46$ for NO_2; and $m/e = 41$ for C_3H_6. Contribution of N_2O and NO_2 to $m/e = 30$ was determined by comparing relative intensities of the fragment and

parent ions of the calibrated N_2O, NO, and NO_2 pulse responses; contribution of CO_2 to $m/e = 28$ was found to be negligible. The MS profiles of the reactants and products were obtained by multiplying their MS intensities by their calibration factors [13,35]. Product selectivity and gas composition were further determined by using a gas IR cell.

3. Results

3.1. NO/O_2 adsorption on $CuO/\gamma\text{-}Al_2O_3$ at 523 K

Fig. 2 shows in situ IR spectra of adsorbed NO_x produced from flowing the high O_2/NO flow and low O_2/NO flow over $CuO/\gamma\text{-}Al_2O_3$ at 523 K. The exposure of $CuO/\gamma\text{-}Al_2O_3$ to the high O_2/NO flow, shown in Fig. 2a, resulted in the immediate formation of a broad band centered at 1370 cm^{-1} and gaseous NO_2 at 1630 and 1594 cm^{-1} while exposure to the low O_2/NO flow led to the formation of chelating nitro ($Cu^{2+}<^{O}_{O}>N$) at 1251 cm^{-1} first, then gradual formation of a sharp band at 1380 cm^{-1} and chelating bidentate nitrate ($Cu^{2+}<^{O}_{O}>N$–O) at 1570 and 1262 cm^{-1} [34,36–42]. The band centered in the 1370–1380 cm^{-1} region which coincided with that of $Cu(NO_3)_2/\gamma\text{-}Al_2O_3$ was assigned to $Cu^{2+}(NO_3^-)_2$ [34]. The broad band in the region of 1450–1300 cm^{-1} produced from the high O_2/NO flow in Fig. 2a appears to have resulted from the overlap of monodentate nitrate (Cu^{2+}–O–N$<^{O}_{O}$), nitrito (Cu^{2+}–O–N=O), and $Cu^{2+}(NO_3^-)_2$ bands. The observed sequence

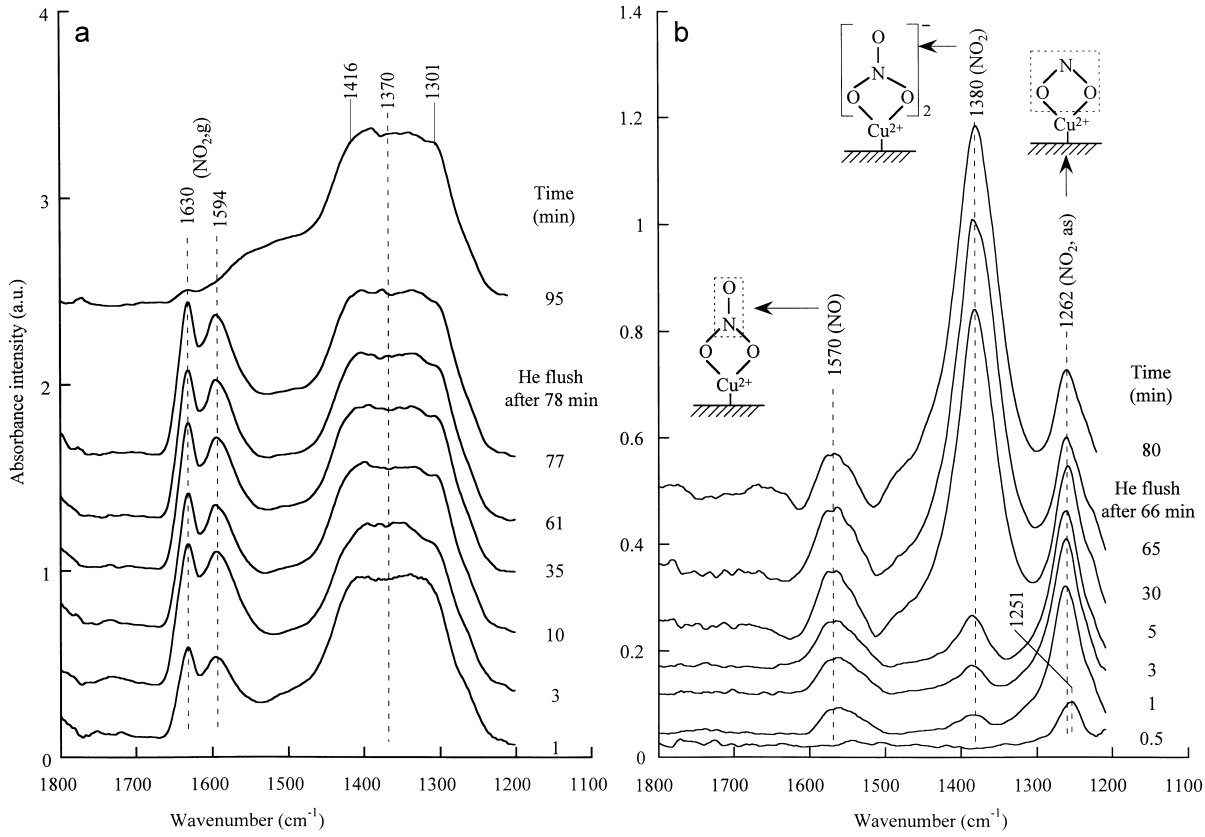

Fig. 2. In situ IR spectra of flowing (a) 0.05% NO + 0.03% NO_2 + 6.66% O_2 + 93.26% He, and (b) 0.08% NO + 2% O_2 + 97.92% He flow over $CuO/\gamma\text{-}Al_2O_3$ at 523 K.

of $Cu^{2+}<^{O}_{O}>N$, $Cu^{2+}<^{O}_{O}>N–O$, and $Cu^{2+}(NO_3^-)_2$ formation in Fig. 2b are consistent with that of our previous study [34] and can be described by the following steps:

$$CuO + NO \Leftrightarrow Cu^{2+}<^{O}_{O}>N \quad (1)$$

$$Cu^{2+}<^{O}_{O}>N + \tfrac{1}{2}O_2 \Leftrightarrow Cu^{2+}<^{O}_{O}>N–O \quad (2)$$

$$Cu^{2+}<^{O}_{O}>N–O + NO + O_2 \Leftrightarrow Cu^{2+}(NO_3^-)_2 \quad (3)$$

$$2Cu^{2+}<^{O}_{O}>N–O + \tfrac{1}{2}O_2 \Leftrightarrow Cu^{2+}(NO_3^-)_2 + CuO \quad (4)$$

It has been reported that NO_2 in the high O_2/NO flow could also contribute to the formation of $Cu^{2+}(NO_3^-)_2$ through interaction of surface oxygen [32,34]. The formation of the broad $Cu^{2+}(NO_3^-)_2$ band in the 1280–1450 cm^{-1} could be attributed in part to the reaction of adsorbed NO_2 with surface oxygen:

$$Cu^{+} \text{or } Cu^{2+} + 2NO_2 + O_2 \Leftrightarrow Cu^{2+}(NO_3^-)_2 \quad (5)$$

CO adsorption studies prior to NO/O_2 and NO_2/O_2 adsorption showed that CuO/γ-Al_2O_3 contained both Cu^{+} and Cu^{2+} sites [34]. The rapid formation of $Cu^{2+}(NO_3^-)_2$ did not allow elucidation of the detailed steps involved in its formation.

Fig. 3a and b show in situ IR spectra of adsorbed NO_x produced from the high O_2/NO and low O_2/NO flow over CuO/γ-Al_2O_3 for 1 h at various temperatures, respectively. $Cu^{2+}(NO_3^-)_2$ at 1365 cm^{-1} was observed for all of experimental conditions, except for the high O_2/NO flow at 298 K. Exposure of CuO/γ-Al_2O_3 to the high O_2/NO flow at 298 K produced gaseous N_2O_4 at 1750 and 1260 cm^{-1} [43],

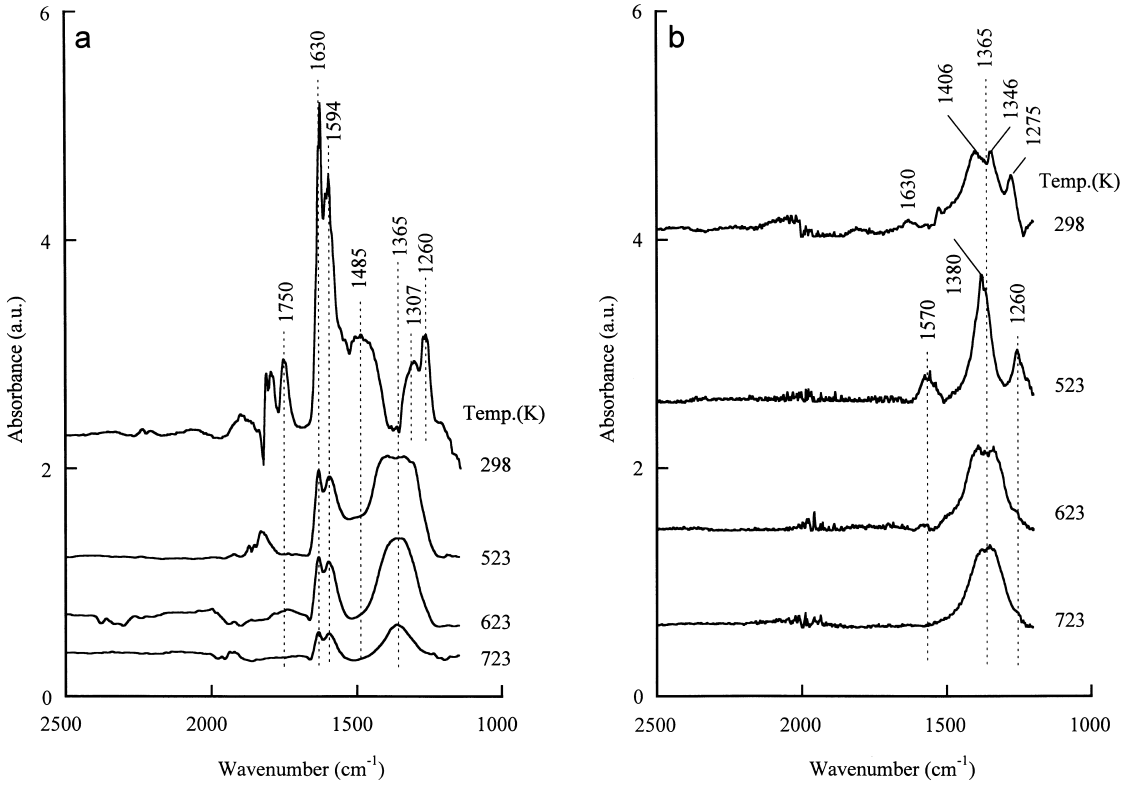

Fig. 3. In situ IR spectra of (a) 0.05% NO + 0.03% NO_2 + 6.66% O_2 + 93.26% He, and (b) 0.08% NO + 2% O_2 + 97.92% He flow over CuO/γ-Al_2O_3 at various temperatures.

NO_2 at 1630 and 1594 cm^{-1}, monodentate nitrate (Cu^{2+}–O–N<O O) at 1485 and 1307 cm^{-1} [34,36,37], and Cu^{2+}<O O>N at 1260 cm^{-1} [34] overlapping with gaseous N_2O_4. Cu^{2+}<O O>N–O was overlapping with gaseous NO_2 in the region of 1630–1570 cm^{-1}. The observation of the intense NO_2 IR band indicates that Cu catalyzed the NO_2 formation for the reaction of NO with O_2 at 298 K. The absence of $Cu^{2+}(NO_3^-)_2$ at 298 K indicates that the sequence of Eqs. (1), (2), (3), (4) for $Cu^{2+}(NO_3^-)_2$ formation did not occur. The formation of $Cu^{2+}(NO_3^-)_2$ from $NO/NO_2/O_2$ appeared to be an activated process, occurring at temperatures above 520 K: its intensity decreased with increasing temperature. Increasing temperature only caused a slight decrease in the IR intensity of $Cu^{2+}(NO_3^-)_2$ for the low O_2/NO flow.

3.2. Pulsing C_3H_6 into the steady-state NO/O_2 flow (pulse SCR) over CuO/γ-Al_2O_3

Fig. 4 shows the MS profiles and in situ IR spectra during pulsing three consecutive 1-cm^3 C_3H_6 pulses into the steady-state high O_2/NO flow over CuO/γ-Al_2O_3 at 623 K. Pulsing C_3H_6 decreased NO, O_2, and NO_2 MS intensity (i.e. concentration) and increased N_2, CO_2, N_2O, and H_2O concentration, indicating occurrence of the conversion of C_3H_6, NO, O_2, and NO_2 to N_2, CO_2, N_2O, and NO. Fig. 4b shows that pulsing C_3H_6 also decreased the IR intensities of

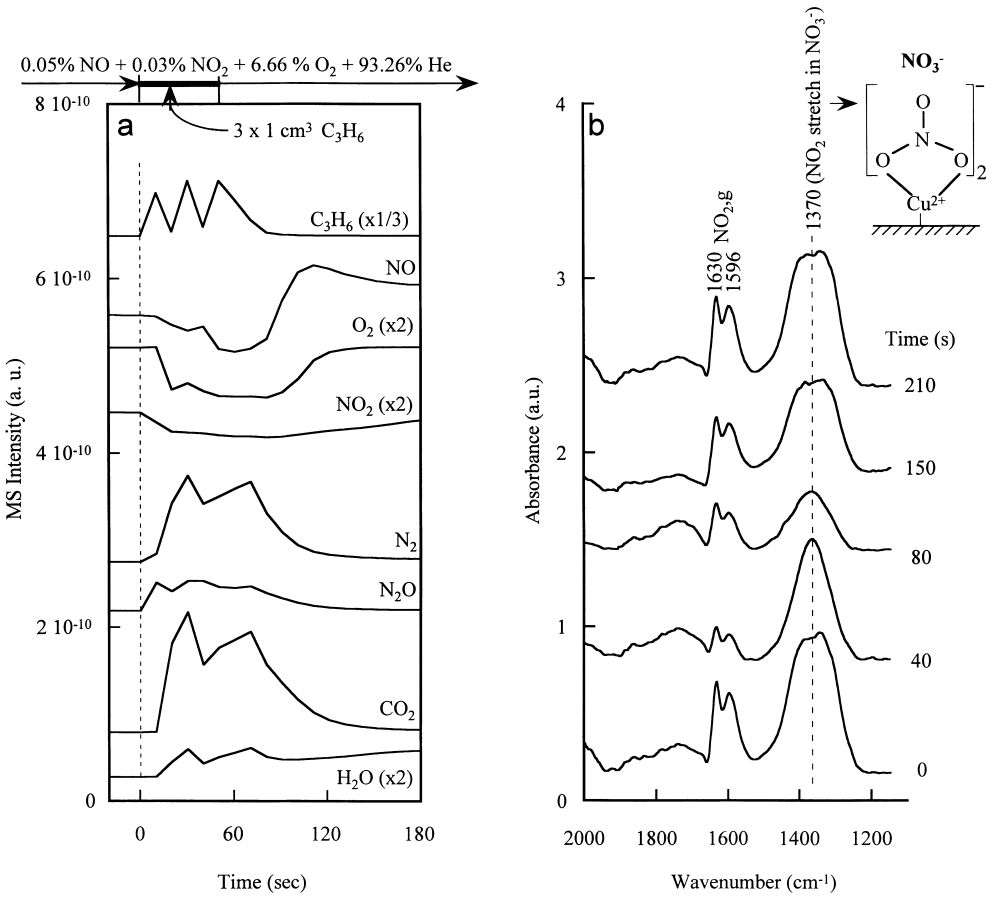

Fig. 4. (a) MS intensity profiles, and (b) in situ IR spectra during pulsing C_3H_6 into the steady-state high O_2/NO flow over CuO/γ-Al_2O_3 at 623 K.

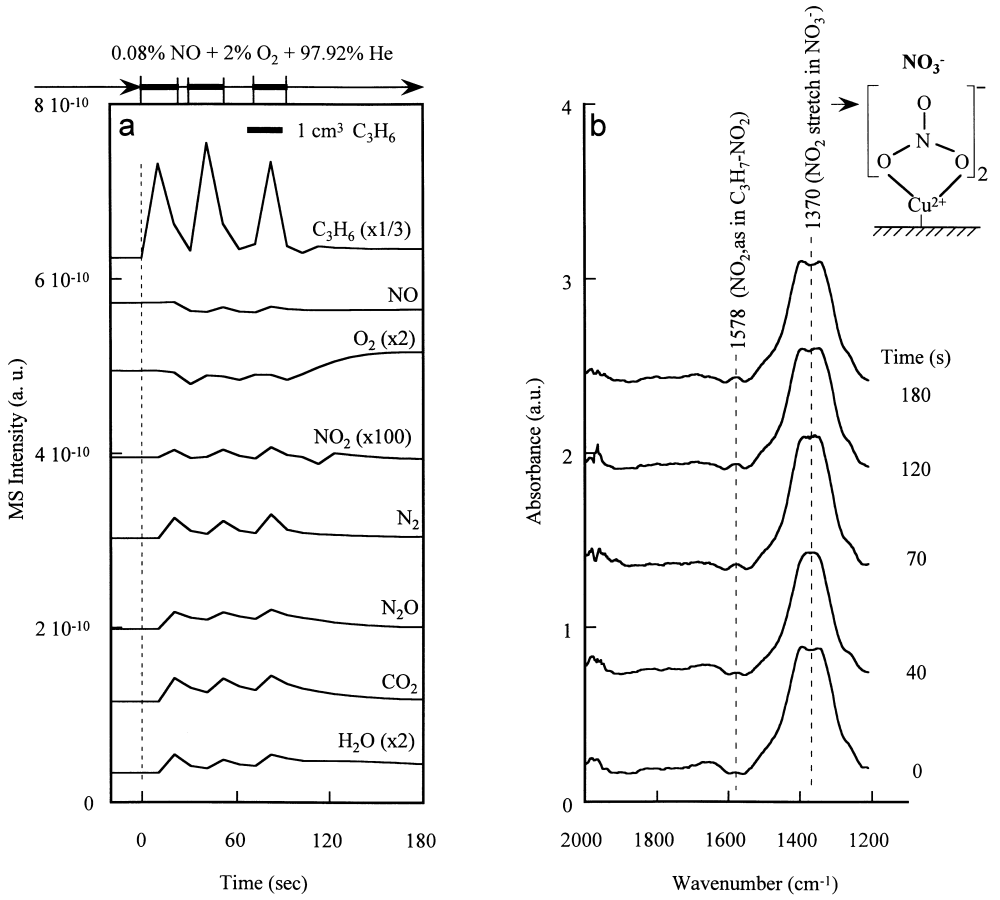

Fig. 5. (a) MS intensity profiles, and (b) in situ IR spectra during pulsing C_3H_6 into the steady-state low O_2/NO flow over CuO/γ-Al_2O_3 at 623 K.

both adsorbed $Cu^{2+}(NO_3^-)_2$ and gaseous NO_2, indicating that they are the active species responsible for product formation. The IR spectrum at 40 s in Fig. 4b corresponds to the concentration of reactant/product in the MS profiles at 40 s in Fig. 4a. The close examination of the lead/lag relationships of the MS product profiles in Fig. 4a showed that the concentration changes in C_3H_6, NO_2, N_2O led to that of N_2 and NO which further led to that of O_2, CO_2, and H_2O; Fig. 3b showed that the decrease in IR intensity of NO_2 led that of $Cu^{2+}(NO_3^-)_2$, suggesting occurrence of the reaction sequence as shown in Fig. 11a.

Results of pulsing C_3H_6 into the low O_2/NO flow, shown in Fig. 5, was plotted in the same scale as those for pulsing C_3H_6 into the high NO/O_2 flow. The absence of NO_2 in the steady-state low O_2/NO flow eliminates the participation of NO_2 in $Cu^{2+}(NO_3^-)_2$ formation. The significant delay in NO and O_2 profiles to those of other gaseous products suggests that N_2, N_2O, NO_2, CO_2, and H_2O were produced from the reaction of C_3H_6 with $Cu^{2+}(NO_3^-)_2$ to create free $Cu^0/Cu^+/Cu^{2+}$ sites for NO and O_2 adsorption and reaction. Comparison of MS profiles and adsorbate intensities in Figs. 4 and 5 shows that pulsing C_3H_6 into the low O_2/NO flow gives lower NO conversion as well as lower rate of product formation than pulsing C_3H_6 into the high O_2/NO flow.

Figs. 6 and 7 compare the effect of temperature on the MS and IR intensity profiles during pulsing three consecutive 1-cm^3 C_3H_6 pulses into the

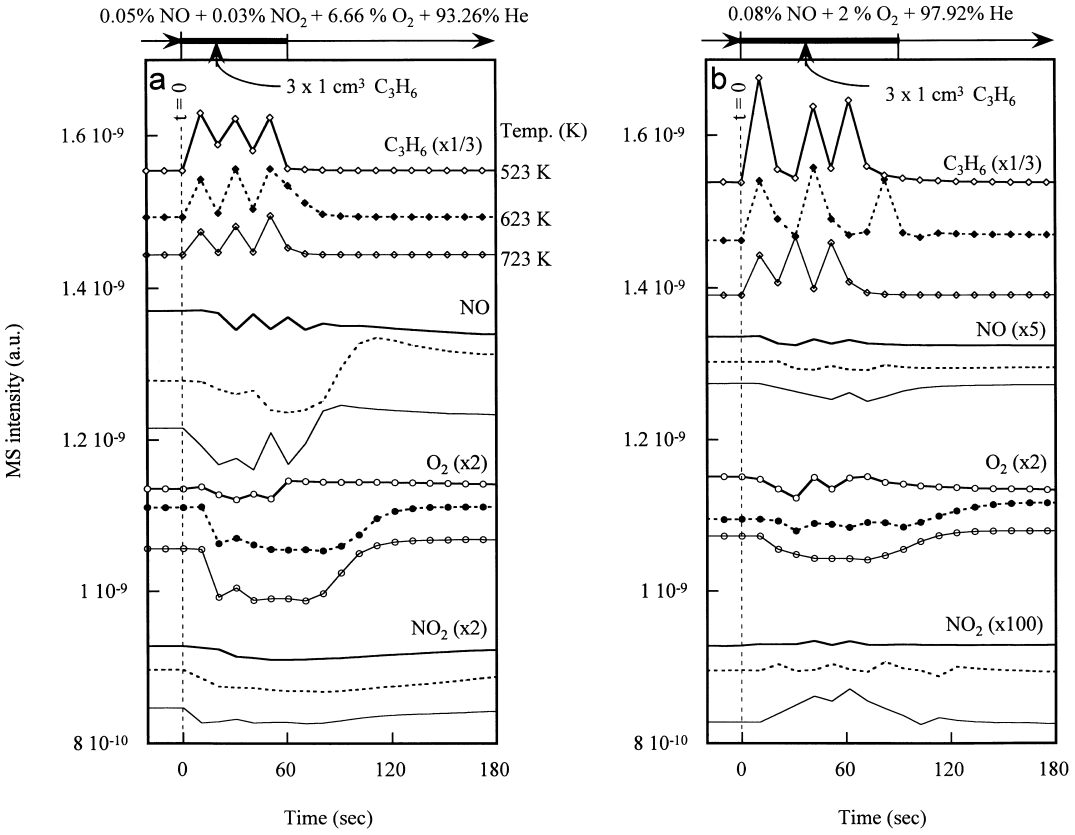

Fig. 6. Reactant MS intensity profiles during pulsing C_3H_6 into the steady-state (a) high O_2/NO flow, and (b) low O_2/NO flow over CuO/γ-Al_2O_3 at various temperatures.

steady-state high O_2/NO flow and low O_2/NO flow over CuO/γ-Al_2O_3. Reactant profiles are presented in Fig. 6 and product profiles are shown in Fig. 7. Increasing temperature, in general, increased the rate of reactant conversion and product formation as evidenced by the increase in the slope of reactant and product MS profiles. The extent of decrease in the IR intensity profiles of adsorbed $Cu^{2+}(NO_3^-)_2$ versus time corresponded approximately to the amount of increase in the MS intensity profiles of N_2, N_2O, CO_2, and H_2O formation in Figs. 6 and 7, further confirming the involvement of $Cu^{2+}(NO_3^-)_2$ in product formation. Adsorbed $Cu^{2+}(NO_3^-)_2$ reacted with C_3H_6 in the presence, and absence, of NO/O_2/NO_2.

Table 1 summarizes the conversion of C_3H_6 and the amount of N_2, N_2O, and CO_2 produced during pulsing three consecutive 1 cm^3 of C_3H_6 into the steady-state high O_2/NO flow and low O_2/NO flow. The high O_2/NO flow gave a higher C_3H_6 conversion, produced a higher ratio of N_2/CO_2, and resulted in a higher product formation rate than the low O_2/NO flow.

3.3. Steady-state SCR reaction of NO/O_2/C_3H_6 on CuO/γ-Al_2O_3

Fig. 8 shows the conversion and N_2 selectivity as a function of temperature during flowing the high O_2/NO reactant stream and the low O_2/NO reactant stream over CuO/γ-Al_2O_3. Increasing temperature increased C_3H_6, NO, NO_2, and O_2 conversion, and N_2 selectivity in the range of 523–773 K. Further increasing temperatures above 773 K could decrease NO conversion and N_2 selectivity due to the dominance of C_3H_6 oxidation at high temperatures [14,44]. Increasing O_2 concentration caused the NO and C_3H_6 con-

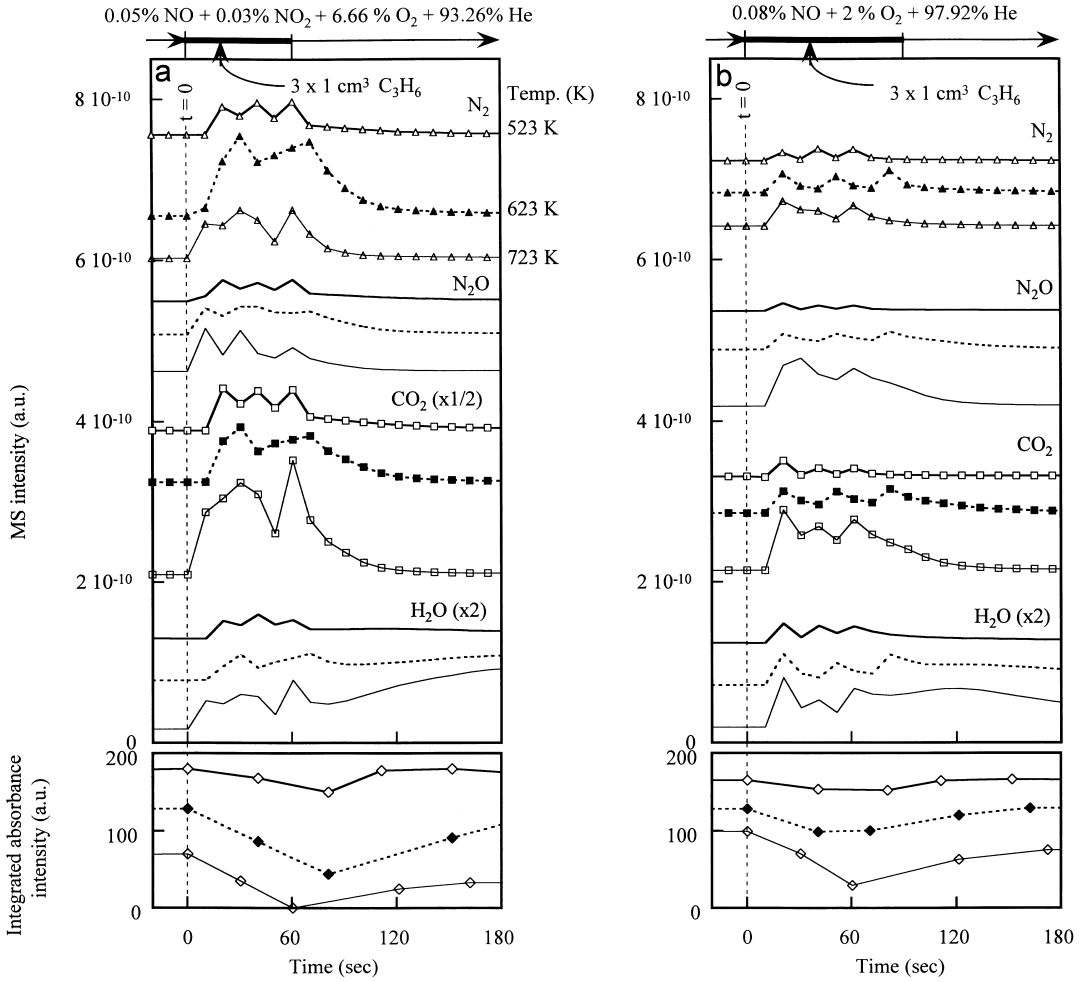

Fig. 7. Product MS intensity profiles and integrated absorbance intensity of $Cu^{2+}(NO_3^-)_2$ during pulsing C_3H_6 into the steady-state (a) high O_2/NO flow, and (b) low O_2/NO flow over CuO/γ-Al_2O_3 at various temperatures.

Table 1
C_3H_6 conversion and product amount during the pulse SCR over CuO/Al_2O_3 at various temperatures

Stream	Temperature (K)	C_3H_6 conversion (%)	Product amount (μmol)[a]		
			N_2	N_2O	CO_2
High O_2/NO flow	523	2.1	0.6	0.4	7.2
	623	2.9	3.2	1.0	11.2
	723	5.8	1.9	1.2	24.3
Low O_2/NO flow	523	0.2	0.2	<0.1	1.0
	623	1.1	0.5	0.4	4.6
	723	3.0	0.7	0.5	12.1

[a] Total amount during pulsing three consecutive 1 cm^3 C_3H_6.

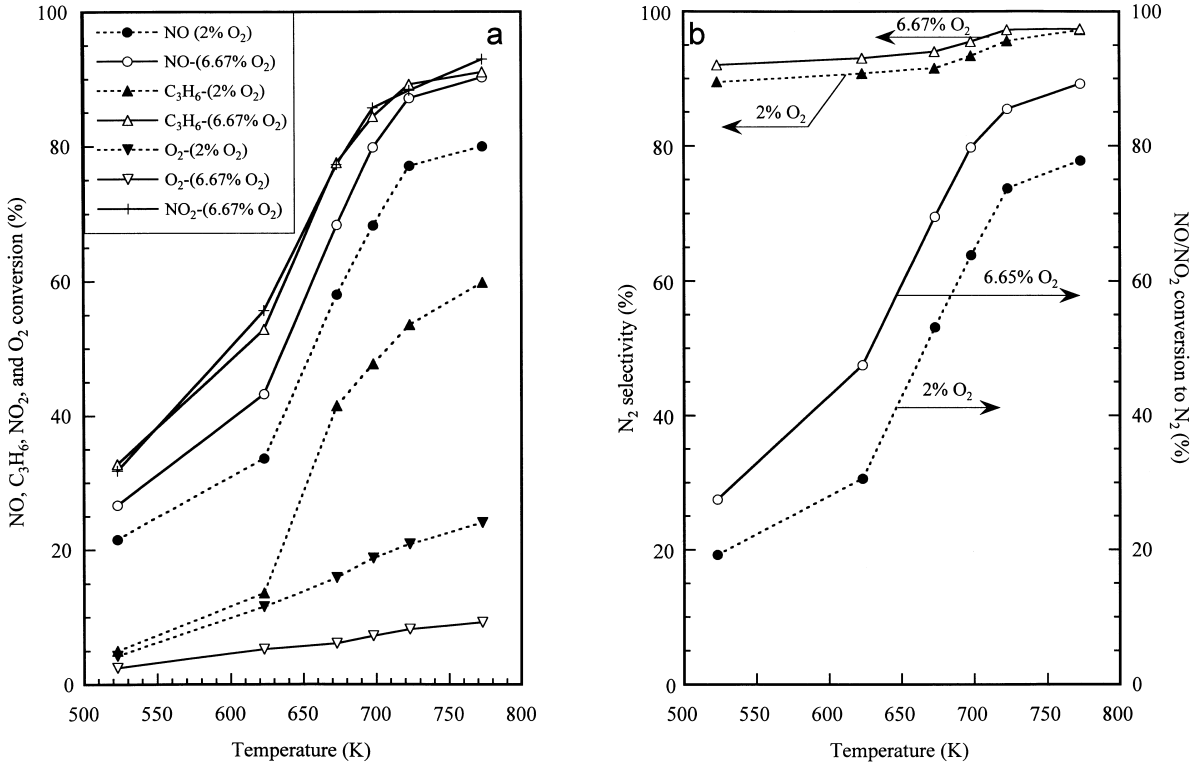

Fig. 8. (a) conversion vs. temperature, and (b) N_2 selectivity ($2 \times \text{mol}\,N_{2\ \text{outlet}} \times 100/\{2 \times \text{mol}\,(N_2 + N_2O)_{\text{outlet}} + \text{mol}\,NO_{2\ \text{outlet}}\}$) and NO/NO_2 conversion to N_2 vs. temperature during the steady-state SCR reaction of $NO/O_2/C_3H_6$ over $CuO/\gamma\text{-}Al_2O_3$.

version to increase. NO/NO_2 conversion in Fig. 8b is the sum of the individual NO and NO_2 conversions.

Fig. 9 shows in situ IR spectra during the steady-state SCR reaction on $CuO/\gamma\text{-}Al_2O_3$ in the 523–773 K range. The IR spectra of the low O_2/NO steady-state SCR reaction at 523 and 723 K have been reported elsewhere [34] and were included in Fig. 9 for comparison. Low O_2/NO steady-state SCR at 523 K produced distinct infrared bands for organic nitro-compound (C_3H_7–NO_2) at 1593 and 1340 cm^{-1}, an organic nitrito-compound (C_3H_7–ONO) at 1662 cm^{-1}, an acetic ion (CH_3COO^-) at 1593 and 1460 cm^{-1} [27,34,45–50], and Cu^+–NCO at 2237 cm^{-1} [12,51,52]. The band at 1593 cm^{-1} was attributed to the overlap of adsorbed C_3H_7–NO_2 with CH_3COO^-. Assignment of C_3H_7–NO_2 and CH_3COO^- bands is verified by adsorption studies of $^{15}N^{18}O/^{14}N^{16}O/C_3H_6$, which will be further discussed in Fig. 10. The IR bands at 1662 and 1460 cm^{-1} are in the range of those for bicarbonate and carbonate as demonstrated by CO_2 adsorption at 523 K. Since these carbonates are not thermally stable at temperature above 550 K, their contribution to the IR spectra in the 1400–1700 cm^{-1} region is expected to significantly decrease as temperature increased. Increasing temperature to 673 K caused an increase in the intensities of CO_2 at 2358 and 2309 cm^{-1} and OH band at 3735 cm^{-1}, a decrease in the intensities of the =C–H and –C–H stretching bands, and a shifted band from 1593 to 1560 cm^{-1}. The contour of the bands in the 1400–1650 cm^{-1} for both low and high O_2/NO SCR were very similar at temperatures above 723 K. A further increase in temperature caused CO_2 intensity to continue increasing, but led the IR bands at 1560 and 1460 cm^{-1} to decrease. The lack of Cu^+–CO and Cu^0–CN in the high O_2/NO reactant flow can be attributed to their oxidation to CO_2 and reduction to N_2 in the presence of high O_2 concentration (6.66%).

Fig. 10 shows in situ IR spectra of C_3H_6 adsorption followed by either NO or $^{15}N^{18}O$ addition on

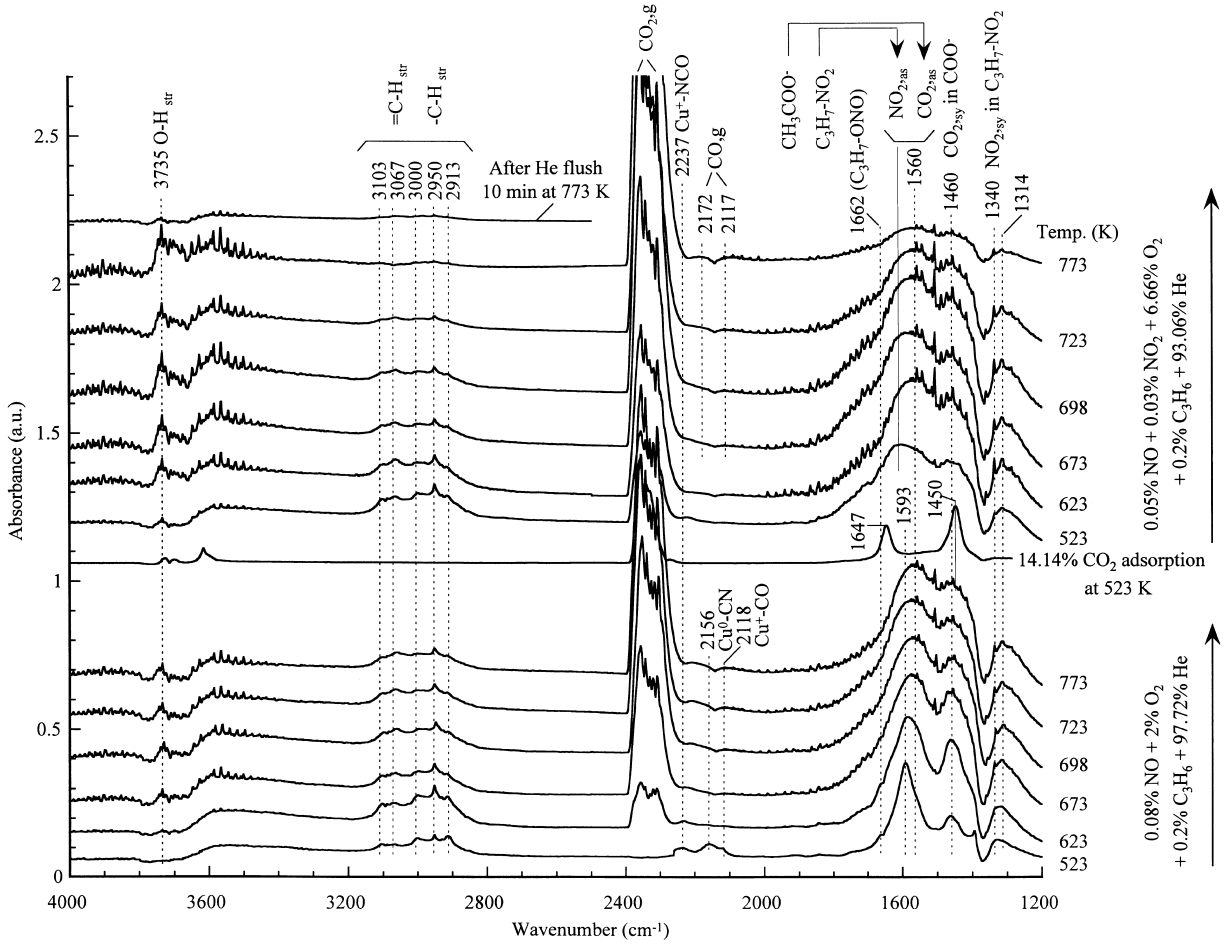

Fig. 9. In situ IR spectra during the steady-state high O_2/NO and low O_2/NO SCR reactant flow over CuO/γ-Al_2O_3 at various temperatures.

CuO/γ-Al_2O_3 at 523 K. To avoid the oxidation of adsorbed intermediates produced from $^{14}N^{16}O/^{15}N^{18}O$ and C_3H_6, O_2 was not included in the adsorption study. Exposure of CuO/γ-Al_2O_3 to C_3H_6 produced adsorbed CH_3COO^- at 1592 and 1460 cm^{-1} and $HCOO^-$ at 1392 cm^{-1} [27,34,45–50,53]. The bands at 1592 and 1460 cm^{-1} were assigned to asymmetric and symmetric stretching mode of $C<^{O^-}_{O}$ in adsorbed CH_3COO^-, respectively. Adsorption of NO on CuO/γ-Al_2O_3 covered with preadsorbed C_3H_6 produced the prominent IR bands at 2236 and 1592 cm^{-1}. These bands shifted to 2223 and 1582 cm^{-1}, respectively, for $^{15}N^{18}O$ adsorption on CuO/γ-Al_2O_3 with preadsorbed C_3H_6, indicating that these bands are resulted from these species containing N and/or NO. Thus, the band which shifted from 1592 to 1582 cm^{-1} is not due to formate species. This observation combined with the band assignment from literature [12,51,52] allowed us to conclude that the band at 1592 $cm^{-1}$is due to C_3H_7–NO_2; the band at 2236 cm^{-1} is due to Cu^+–NCO.

4. Discussion

4.1. Reaction mechanism of NO SCR

The significant difference in the type of adsorbates observed for the pulse SCR in Figs. 4 and 5 and the

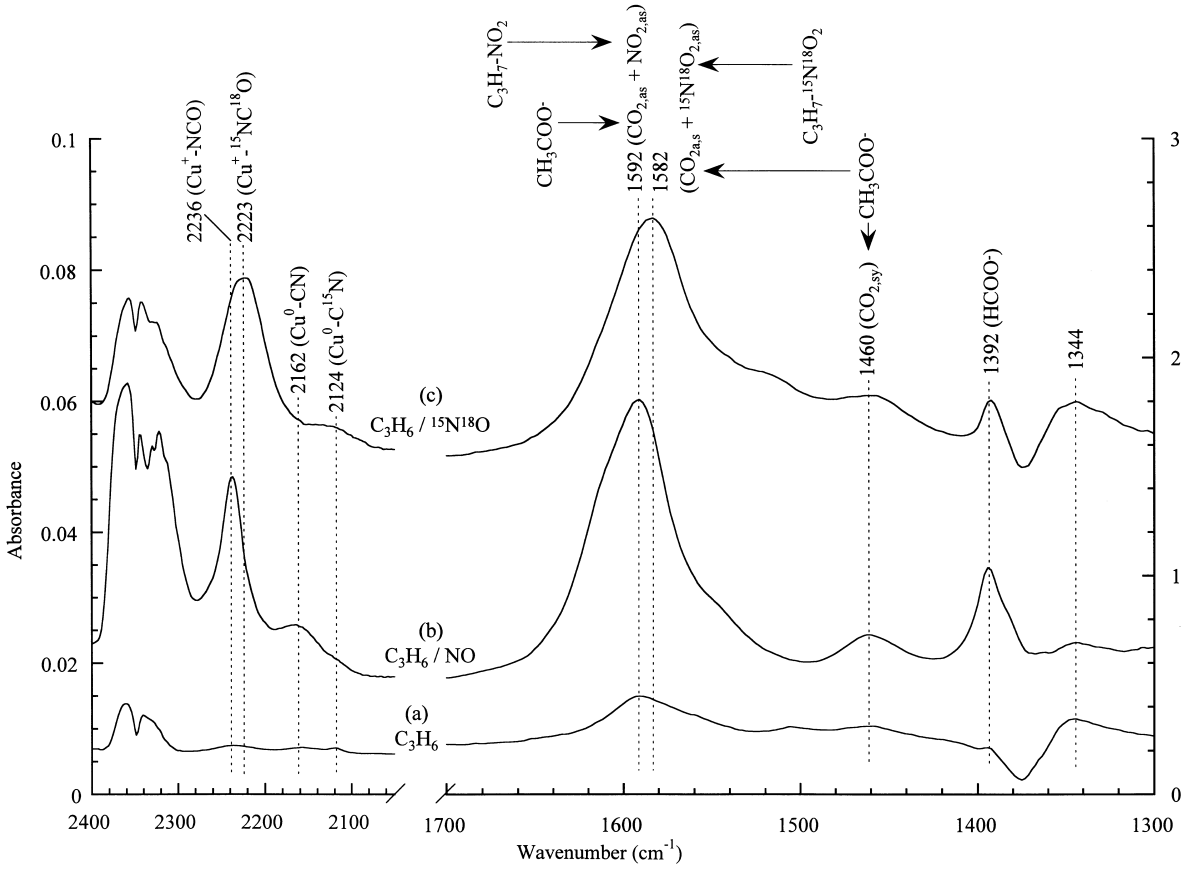

Fig. 10. In situ IR spectra of (a) 0.2% C_3H_6 adsorption for 20 min, followed by addition of (b) NO, and (c) $^{15}N^{18}O$ for 1 min on $CuO/\gamma\text{-}Al_2O_3$ at 523 K.

steady-state SCR in Fig. 9 clearly demonstrates that the pulse SCR and the steady-state SCR follow different reaction pathways. Fig. 11a shows the proposed reaction pathway for the pulse SCR on $CuO/\gamma\text{-}Al_2O_3$ according to the observed sequence of adsorbate and product formation. The proposed pathway includes: (i) the oxidation of Cu^0/Cu^+ to Cu^{2+} by NO and O_2; (ii) the co-adsorption of $NO/NO_2/O_2$ to produce $Cu^{2+}(NO_3^-)_2$; and (iii) the reaction of $Cu^{2+}(NO_3^-)_2$ with C_3H_6 to produce N_2, CO_2, and H_2O. Steps (i) and (ii), the abbreviated versions of Eqs. (1), (2), (3) and (4), were first established by our earlier studies [34] and supported by the formation of $Cu^{2+}(NO_3^-)_2$ as shown in Fig. 2. The similarity in the contour of the infrared bands (shown in Fig. 2) produced from both high and low O_2/NO flow at temperatures above 623 K suggests the presence of rapid equilibrium among NO, NO_2, and O_2, allowing the formation of very similar $Cu^{2+}(NO_3^-)_2$ infrared bands. At 723 K, $Cu^{2+}(NO_3^-)_2$ produced from the high O_2/NO flow in Fig. 3a and the low O_2/NO flow in Fig. 3b gave the similar Gaussian shape of bands, suggesting that the identical $Cu^{2+}(NO_3^-)_2$ was produced. The presence of this intense IR band at 723 K suggests that its formation rate from steps (1)–(5) is higher than the rate of its destruction (i.e. the reverse step) and further revealed that $CuO/\gamma\text{-}Al_2O_3$ catalyst can serve as an effective adsorbent for NO/O_2 at 723 K.

The involvement of $Cu^{2+}(NO_3^-)_2$ in the reaction with C_3H_6 is evidenced by the consumption of $Cu^{2+}(NO_3^-)_2$ and the formation of N_2 and CO as shown in Figs. 4 and 5. However, no information

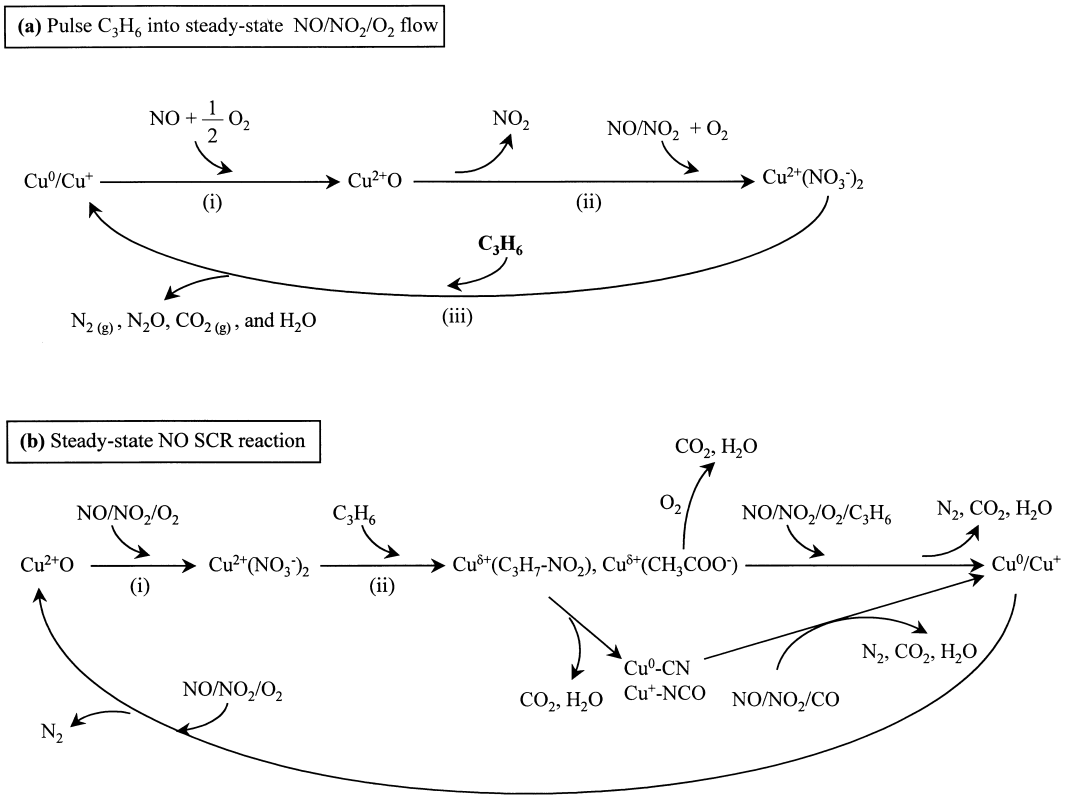

Fig. 11. Proposed pathway for (a) the reaction between adsorbed $(NO_3^-)_2$ and C_3H_6 pulse, and (b) the steady-state NO SCR with C_3H_6 in the presence of O_2 over $CuO/\gamma\text{-}Al_2O_3$.

on the involvement of adsorbed C_3H_6 can be obtained from our infrared studies due to the absence of IR-observable adsorbed hydrocarbon species, resulting from the rapid reaction between adsorbed C_3H_6 and $Cu^{2+}(NO_3^-)_2$. Furthermore, C_3H_6 is a limiting reactant under conditions of pulsing C_3H_6 into the NO/O_2 flow, leading to a rapid depletion of adsorbed C_3H_6.

Fig. 11b illustrates the proposed reaction pathway for the steady-state NO SCR on $CuO/\gamma\text{-}Al_2O_3$. The steady-state SCR reaction may proceed via a number of infrared-observable intermediates: adsorbed C_3H_7–NO_2, C_3H_7–ONO, CH_3COO^-, and Cu^+–NCO (shown in Fig. 9). Our previous studies [34] showed that these species responded rapidly to the change in concentration of reactants, exhibiting the typical transient nature of reaction intermediates. It has been recently reported that the rate of disappearance for CH_3COO^-, generated from the stream of $NO + C_3H_6 + O_2$ over Al_2O_3, under $NO + O_2$ flow is in the same order of magnitude as that of NO SCR, further supporting the role of CH_3COO^- in the SCR [14]. The question of whether these observed species adsorbed on Al_2O_3 or $CuO/\gamma\text{-}Al_2O_3$ is yet to be answered. Due to the lack of techniques to observe the intermediates between reactants/products and the IR-observable species, the steps proposed for the conversion of reactants to C_3H_7–NO_2, C_3H_7–ONO, CH_3COO^-, and Cu^+–NCO as well as that of these species to products remain highly speculative.

The difference in reaction pathway for the pulse SCR and steady-state SCR is evidenced by not only the different types of adsorbates, but also the distinction in Cu surface states. CO adsorption studies [34] show that the pulse SCR resulted in mainly Cu^{2+} on the $CuO/\gamma\text{-}Al_2O_3$ surface while the steady-state SCR led to more Cu^+ than Cu^{2+} sites. Although the concentration of C_3H_6 is significantly less than that of O_2,

the continuous presence of C_3H_6 in the steady-state SCR reactant flow allowed to keep a significant fraction of Cu in the Cu^+ state, minimizing the concentration of NO_x species on the surface.

4.2. Role of O_2 in NO SCR

Increasing O_2 concentration in both pulse and steady-state SCR caused the conversions of NO and C_3H_6 to increase. The possible roles of oxygen include activation of C_3H_6 [23,54], oxidation of NO to NO_2 [26], maintenance of the Cu^+/Cu^{2+} site balance [24], conversion of carbonaceous and alkyl intermediates to CO_2 and N_2 [30–32]. Since the adsorbed oxygen on the catalyst surface cannot be observed by infrared spectroscopy, its role in the reaction has to be elucidated from its interaction with NO and C_3H_6 and the resulting intermediates and products, which can be observed by IR and MS. Increasing oxygen concentration led to an immediate formation of NO_2 and $Cu^{2+}(NO_3^-)_2$ during NO/O_2 coadsorption (shown in Fig. 1) and increase in $NO/NO_2/C_3H_6$ conversion during the pulse SCR. These results revealed that during pulse SCR, high oxygen concentration accelerates the formation of NO_2 and $Cu^{2+}(NO_3^-)_2$, enhancing the rate of $NO_2/Cu^{2+}(NO_3^-)_2$ reaction with C_3H_6. Since NO_2 is more reactive toward C_3H_6 than NO [7,19,54], an increase in conversion of NO to NO_2 could also facilitate the conversion of NO to N_2.

The formation of NO_2 from oxidation of NO with O_2 is a thermodynamically favorable process at 303 K. Increasing temperature decreases the equilibrium yield of NO_2. There are a number of pathways for NO_2 formation from NO/O_2: (a) gas phase oxidation of NO [55]; (b) catalytic oxidation of NO; and (c) the reaction between $NO/O_2/C_3H_6$. Each of these types of reactions occurred to a significant extent at specific conditions. Gas phase oxidation took place with a NO conversion of 37.5% in the high O_2/NO (the ratio of $O_2/NO = 83.4$) flow at 298 K. The NO in the high O_2/NO flow was further oxidized to NO_2 over $CuO/\gamma\text{-}Al_2O_3$ at 298 K (shown in Fig. 2a). Both gas phase and catalytic oxidation of NO did not occur in the low O_2/NO (the ratio of $O_2/NO = 25.0$) flow. We have further found that allowing the low O_2/NO ratio gas to mix for >2 min also resulted in the formation of appreciable amount of NO_2 at 298 K; however, we did not determine the kinetics and rate law of NO_2 formation. Formation of NO_2 from pulsing C_3H_6 into the low O_2/NO flow at 523, 623, and 723 K may proceed via the following steps:

$$CH_3\text{–}CH{=}CH_2 \xrightarrow{+O_2} CH_3CH_2COO$$

$$CH_3CH_2OO + NO \rightarrow CH_3CH_2CO + NO_2$$

The increase in NO_2 formation with temperature during pulsing C_3H_6 into the low O_2/NO flow observed in Fig. 6b can be explained by increase in the rate of the above steps with temperature. Variation of C_3H_6 concentration during the C_3H_6 pulse may limit the complete oxidation of C_3H_6, allowing its partially oxidized intermediates to react with NO. No experimental evidence is available for determining whether this reaction took place in either the homogeneous gas phase or the heterogeneous catalyst surface.

The role of C_3H_6 as a limiting reactant under the conditions of the pulse SCR allowed $Cu^{2+}(NO_3^-)_2$ to dominate the catalyst surface. In contrast, steady-state SCR conditions allowed C_3H_6 to keep a significant fraction of Cu in the Cu^+ state and allowed C_3H_7–NO_2, C_3H_7–ONO and CH_3COO^- to dominate the catalyst surface. Fig. 9 shows that increasing oxygen concentration broadened the bands for C_3H_7–NO_2, C_3H_7–ONO, and CH_3COO^- and decreased significantly their intensities at temperature above 723 K. The latter confirmed the role of oxygen in conversion of carbonaceous and intermediates to CO_2 and N_2. The similarity in the contour of the infrared bands in the 1200–1800 cm^{-1} region (shown in Fig. 9) produced from both high and low O_2/NO steady-state SCR flow at temperatures above 673 K suggests the presence of rapid equilibrium among NO, NO_2, and O_2 and their reaction with adsorbed C_3H_6 species, allowing the formation of C_3H_7–NO_2, C_3H_7–ONO, and CH_3COO^-. However, the specific reaction pathway between $NO/NO_2/O_2$ and C_3H_6 cannot be simply elucidated from our infrared studies.

In general, the presence of O_2 in NO and NO_2 flow increased the rate of conversion of C_3H_6 [14]. Increasing temperature from 523 to 723 K increases the conversion of C_3H_6 and the formation of CO_2, N_2O, and N_2. The exception observed for N_2 formation from 623 to 723 K at the high O_2/NO flow during the pulse SCR in Table 1 is due to the dominance of oxidation of C_3H_6 over reduction of NO by C_3H_6.

Previous studies have found that the presence of O_2 in NO/NO_2 flow enhanced the rate of the formation of $Cu^{2+}(NO_3^-)_2$, Cu nitrate, on Cu–ZSM-5 [29] and CuO/γ-Al_2O_3 [34]. The absence of such a nitrate species in the steady-state SCR suggests that the nitrate may be rapidly depleted by the reaction with C_3H_6 to produce C_3H_7–NO_2, C_3H_7–ONO, and CH_3COO^- (Step (ii) in Fig. 11b). Thus, we suggest that increasing O_2 concentration in the steady-state SCR may accelerate the rates of both C_3H_7–NO_2, C_3H_7–ONO, and CH_3COO^- formation and their disappearance, increasing $NO/O_2/C_3H_6$ conversion, but maintaining nearly constant intensities for these adsorbed species in the 523–698 K range (shown in Fig. 9). The rate of disappearance for these species through oxidation began dominating at temperatures above 723 K where a substantial decrease in their IR intensities with temperature were observed for the high O_2/NO SCR.

5. Conclusions

Infrared spectroscopy coupled with mass spectroscopic studies of the pulse and steady-state SCR provides insight into the reaction pathway, the role of oxygen, and its concentration effect on the reaction. The pulse SCR proceeds via: (i) the oxidation of Cu^0/Cu^+ to Cu^{2+} by NO and O_2; (ii) the co-adsorption of $NO/NO_2/O_2$ to produce $Cu^{2+}(NO_3^-)_2$; and (iii) the reaction of $Cu^{2+}(NO_3^-)_2$ with C_3H_6 to produce N_2, CO_2, and H_2O. Increasing the O_2/NO ratio from 25.0 to 83.4 promotes the formation of NO_2 from gas phase oxidation of NO, resulting in a reactant mixture of $NO/NO_2/O_2$. This reactant mixture allows the formation of $Cu^{2+}(NO_3^-)_2$ and its reaction with the C_3H_6 to occur at a higher rate with a higher selectivity toward N_2 than the low O_2/NO flow. Thus, the kinetics of NO_2 formation form NO/O_2 plays a significant role in the pulse SCR. The accurate measurement of $NO/NO_2/O_2$ concentration in the reactant flow is essential for the pulse SCR study.

The role of NO_2 is less significant in the steady-state SCR than the pulse SCR. The presence of NO_2 in the $NO/O_2/C_3H_6$ stream did not alter the steady-state SCR reaction pathway. High O_2 concentration in the high O_2/NO steady-state SCR accelerates both formation and destruction of adsorbed C_3H_7–NO_2, C_3H_7–ONO, and CH_3COO^- intermediates, resulting in their intensities similar to the low O_2/NO steady-state SCR at 523, 623, 673, and 698 K. High O_2 concentration in the reactant mixture resulted in a higher the rate of destruction of the intermediates than low O_2 concentration at temperature above 723 K.

Acknowledgements

Although the research described in this article has been funded wholly by the United States Environmental Protection Agency under assistant agreement R823529-01-0 to the University of Akron, it has not been subject to the Agency's peer and administrative review and, therefore, may not necessary reflect the views of the Agency, and no official endorsement should be inferred.

References

[1] M. Shelef, Chem. Rev. 95 (1995) 209.
[2] M. Iwamoto, Catal. Today 29 (1996) 29.
[3] V.A. Bell, J.S. Feeley, M. Deeda, R.J. Farrauto, Catal. Lett. 29 (1994) 15.
[4] Y. Li, J.N. Amor, Appl. Catal. B 5 (1995) L257.
[5] T.E. Hoost, K.A. Laframboise, K. Otto, Appl. Catal. B 7 (1995) 79.
[6] A.W. Aylor, S.C. Larson, J.A. Reimer, A.T. Bell, J. Catal. 157 (1995) 592.
[7] B.J. Adelman, T. Beutel, G.-D. Lei, W.M.H. Sachtler, J. Catal. 158 (1996) 327.
[8] D.B. Lukyanov, E.A. Lombardo, G.A. Sill, J.L. d'Itri, W.K. Hall, J. Catal. 163 (1996) 447.
[9] K.A. Bethke, H.H. Kung, J. Catal. 172 (1997) 93.
[10] R. Burch, A.A. Shestov, J.A. Sullivan, J. Catal. 182 (1999) 497.
[11] Y.-H. Yin, A. Pisanu, L. Serventi, W.E. Alvarez, D.E. Resasco, Catal. Today 54 (1999) 419.
[12] D.K. Captain, M.D. Amiridis, J. Catal. 184 (1999) 377.
[13] M.V. Konduru, S.S.C. Chuang, J. Catal. 187 (1999) 436.
[14] F.C. Meunier, J.P. Breen, V. Zuzaniuk, M. Olsson, J.R.H. Ross, J. Catal. 187 (1999) 493.
[15] S. Xie, M.P. Rosynek, J.H. Lunsford, J. Catal. 188 (1999) 24.
[16] M. Iwamoto, N. Mizuno, H. Yahiro, Stud. Surf. Sci. Catal. 75 (1993) 1285.
[17] B. Ganemi, E. Björnbom, J. Paul, Appl. Catal. B 17 (1998) 293.
[18] L.G. Pinaeva, E.M. Sadovakaya, A.P. Suknev, V.B. Goncharov, V.A. Sadykov, B.S. Balzhinimaev, T. Décamp, C. Mirodatos, Chem. Eng. Sci. 54 (1999) 4327.
[19] M.C. Kung, P.W. Park, D.-W. Kim, H.H. Kung, J. Catal. 181 (1999) 1.

[20] M.W. Kumthekar, U.S. Ozkan, J. Catal. 171 (1997) 45.
[21] L.G. Pinaeva, A.P. Suknev, A.A. Budneva, E.A. Paukshtis, B.S. Bal'zhinimaev, J. Mol. Catal. 112 (1996) 115.
[22] R. Bilbao, A. Millera, M.U. Alzueta, Ind. Eng. Chem. Res. 33 (1994) 2846.
[23] G.R. Bamwenda, A. Obuchi, A. Ogata, J. Oi, S. Kushiyama, H. Yagita, K. Mizuno, Stud. Surf. Sci. Catal. 121 (1999) 263.
[24] J.O. Petunchi, W.K. Hall, Appl. Catal. B 2 (1993) L17.
[25] M. Sasaki, H. Hamada, Y. Kintaichi, T. Ito, Catal. Lett. 15 (1992) 3297.
[26] C. Yokoyama, M. Misono, J. Catal. 150 (1994) 9.
[27] J.L. d'Itri, W.M.H. Sachtler, Appl. Catal. B 2 (1993) L7.
[28] I.C. Hwang, D.H. Kim, S.I. Woo, Catal. Today 44 (1998) 47.
[29] V.A. Matyshak, A.A. Ukharskii, A.N. Il'ichev, V.A. Sadykov, V.N. Korchak, Kinet. Catal. 40 (1999) 105.
[30] M. Haneda, Y. Kintaichi, M. Inaba, H. Hamada, Catal. Today 42 (1998) 127.
[31] K.-I. Shimizu, H. Kawabata, A. Satsuma, T. Hattori, J. Phys. Chem. B 103 (1999) 5240.
[32] K. Hadjiivanov, D. Klissurski, G. Ramis, G. Busca, Appl. Catal. B 7 (1996) 251.
[33] N. Takahashi, H. Shinjoh, T. Iijima, T. Suzuki, K. Yamazaki, K. Yokota, H. Suzuki, N. Miyoshi, S.-I. Matsumoto, T. Tanizawa, T. Tanaka, S.-S. Tateishi, K. Kasahara, Catal. Today 27 (1996) 63.
[34] Y. Chi, S.C.C. Chuang, J. Catal. 190 (2000) 75.
[35] S.S.C. Chuang, M.A. Brundage, M.W. Balakos, G. Srinivas, Appl. Spectrosc. 49 (1995) 1151.
[36] K. Nakamoto, Infrared and Raman Spectra of Inorganic and Coordination Compounds, fourth Edn., Wiley, New York, 1986.
[37] A.A. Davydov, Infrared Spectra of Adsorbed Species on the Surface of Transition Metal Oxides, Wiley, Chichester, England, 1990.
[38] J. Laane, J.R. Ohlsen, Progr. Inorg. Chem. 27 (1980) 465.
[39] D.A. Outka, R.J. Madix, Surf. Sci. 179 (1987) 1.
[40] F. Vratny, Appl. Spectrosc. 13 (1959) 59.
[41] C.C. Addison, B.M. Gatehouse, J. Chem. Soc. Feb (1960) 613.
[42] J.R. Ferraro, J. Mol. Spectrosc. 99 (1960) 4.
[43] J.L. Domenech, A.M. Andrews, S.P. Belov, G.T. Fraser, W.J. Lafferty, J. Chem. Phys. 100 (1994) 6993, and references therein.
[44] D.K. Captain, K.L. Roberts, M.D. Amiridis, Catal. Today 42 (1998) 93.
[45] T. Tanaka, T. Okuhara, M. Misono, Appl. Catal. B 4 (1994) L1.
[46] H.Yasuda, T. Miyamoto, M. Misono, in: U.S. Ozkan, S.K. Agarwal, G. Marcelin, (Eds.), Reduction of Nitrogen Oxide Emission, ACS Symposium Ser. No. 587, ACS, Washington, DC, 1995, 110 pp.
[47] N.W. Hayneys, R.W. Joyner, E.S. Shipro, Appl. Catal. B 8 (1996) 343.
[48] A. Satsuma, T. Enjoji, K.-I. Shimizu, K. Sato, H. Yoshida, T. Hattori, J. Chem. Soc. Faraday Trans. 94 (1998) 301.
[49] N.B. Colthup, L.H. Daly, S.E. Wiberley, Introduction to Infrared and Raman Spectroscopy, third Edn., Academic Press, San Diego, CA, 1990.
[50] R.M. Silverstein, F.X. Webster, Spectrometric Identification of Organic Compounds, sixth Edn., Wiley, England, 1997.
[51] F. Radtke, R.A. Koeppel, E.G. Minardi, A. Baiker, J. Catal. 167 (1997) 127.
[52] J. Kiss, F. Solymosi, J. Catal. 179 (1998) 277.
[53] K.-I. Shimizu, H. Kawabata, H. Maeshima, A. Satsuma, T. Hattori, J. Phys. Chem. B 104 (2000) 2885.
[54] M.D. Amiridis, K.L. Roberts, C.J. Pereira, Appl. Catal. B 14 (1997) 203.
[55] J. Smith, J. Phillips, in: J.N. Armor (Ed.), Extended Abstracts of 2nd World Congress on Environmental Catalysis, AIChE Annual Meeting, Miami Beach, FL, USA, November 1998, 12 pp.